Improving structural features of nanoporous alumina using deuterated electrolytes

Anastasia Christoulaki, Chiara Moretti, Alexis Chennevière, Emmanuelle Dubois, Nicolas Jouault

Graphical Abstract

Improving structural features of nanoporous alumina using deuterated electrolytes

Anastasia Christoulaki, Chiara Moretti, Alexis Chennevière, Emmanuelle Dubois, Nicolas Jouault

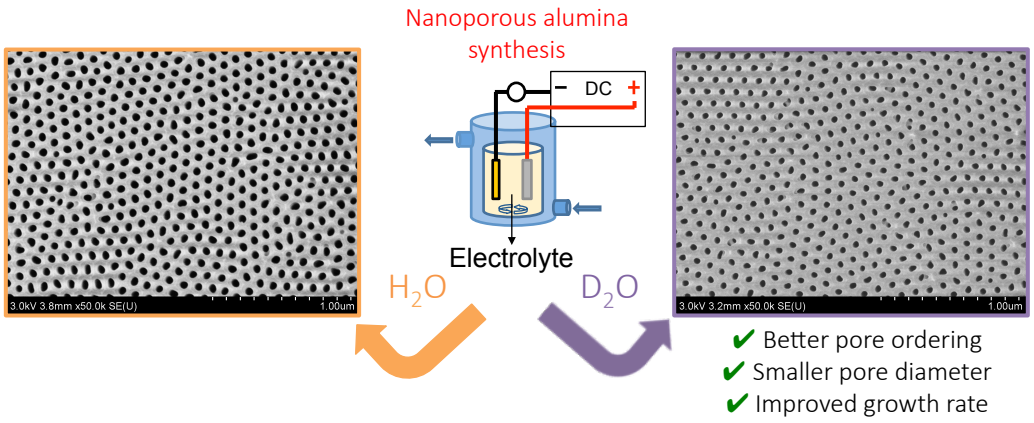

Highlights

Improving structural features of nanoporous alumina using deuterated electrolytes

Anastasia Christoulaki, Chiara Moretti, Alexis Chennevière, Emmanuelle Dubois, Nicolas Jouault

- Nanoporous alumina have been synthesized using deuterated electrolytes.
- The pore diameter reached with deuterated electrolytes is as small as the smallest pore size obtained so far in the literature.
- A better hexagonal pore ordering is observed and correlated to an increase in anion incorporation.
- The pore growth rate is improved and related to a decrease in the activation energy of the alumina formation.
- Thanks to the sensitivity of Small-Angle Neutron Scattering to deuteration, the use of deuterated electrolytes allows discussing the presence or not of OH groups within the material.

Improving structural features of nanoporous alumina using deuterated electrolytes

Anastasia Christoulaki[a], Chiara Moretti[a], Alexis Chennevière[b], Emmanuelle Dubois[a], Nicolas Jouault[a,*]

[a]*Sorbonne Université, CNRS, Laboratoire Physicochimie des Electrolytes et des Nanosystèmes Interfaciaux, PHENIX, F-75005 Paris, France.*
[b]*Laboratoire Léon Brillouin, Université Paris-Saclay, CEA-CNRS, Saclay, 91191 Gif-sur-Yvette CEDEX, France.*

Abstract

Nanoporous anodic aluminum oxides (AAOs) are well-known nanoporous materials with multiple applications. In the last years new experimental strategies have been developed to produce AAOs in order to tune the pore morphology or ordering and discuss the AAOs growth mechanism. Here we describe an original approach to synthesize AAOs using deuterated electrolytes (i.e. sulfuric or oxalic acids in deuterated water D_2O) leading to a pore diameter reduction of around 20 % and an increase in the pore ordering and pore growth. Better pore ordering in D_2O is correlated to an increase in anion incorporation during the synthesis and the growth rate improvement is related to a decrease in the activation energy of the alumina formation. Moreover, the use of deuterated species allows to discuss the incorporation of hydroxyl groups during the AAO synthesis or the hydration after immersion in H_2O or D_2O by Small-Angle Neutron Scattering (SANS), a technique

*Corresponding author
Email address: nicolas.jouault@sorbonne-universite.fr (Nicolas Jouault)

sensitive to deuteration. SANS reveals no changes between AAOs synthesized in H_2O or D_2O due to OH incorporation but shows differences after a long immersion time in water (H_2O or D_2O), indicating that the hydration is a slow process. This work shows that the use of deuterium is an interesting alternative for the synthesis of AAOs with well-controlled and specific morphologies and, from a fundamental point of view, can bring new general understanding about AAOs formation.
Keywords: Nanoporous alumina, Synthesis, Deuterated electrolytes, Pore ordering, Small-Angle Neutron Scattering

1. Introduction

Nanoporous anodic alumina oxides (AAOs) consist of parallel nanochannels with pore diameter (D_p), interpore distance (D_{int}), length (L) and porosity (P) perfectly tunable through the synthesis conditions. Thanks to the versatility of the obtained morphology, AAOs became very popular nanomaterials and are currently used in many applications such as confining medium[1], sensors[2] or templates[3]. AAOs are synthesized by the anodization of pure aluminum in acidic electrolytes under potentiostatic (constant voltage) or galvanostatic (constant current) conditions. In 1995, Masuda and Fukuda proposed an experimental approach to obtain well-ordered nanopores organization thanks to a two-step anodizations synthesis under conventional conditions called "mild anodization" (named MA, corresponding to the use of a moderate temperature and moderate voltage giving a typical growth rate (GR) below 10 μm/h)[4]. Later, hard anodization (HA) was proposed to increase the GR (around 50 μm/h) by making the synthesis with higher

voltage (above the voltage breakdown) by working at low temperature (below 0^oC)[5]. In such conditions, HA usually leads to the formation of larger pores ($>$ 100 nm) and higher interpore distance (from 200 to 500 nm) with, compared to MA, different linear evolution with the voltage[6]. For both MA and HA the classical electrolytes used are sulfuric, oxalic or phosphoric acids but various other dicarboxylic acid electrolytes have been also used such as malonic, tartronic, maleic, tartaric, or citric acids[7].

In the last years, a particular attention has been drawn on the optimization of AAOs synthesis in order to tune the pore morphology, pore ordering and GR. New experimental protocols involving new electrolytes or new anodization conditions have been explored. For example, the smallest pore diameter has been reached by using selenic acid (around 10 nm with low pore density and aspect ratio after 1h anodization)[8] or concentrated sulfuric acid (around 15 nm for higher pore density and a total thickness of 50 μm)[9]. Increasing the electrolyte concentration also leads to an increase of pore self-ordering, as observed for AAOs synthesized with concentrated oxalic acid[10]. Besides, a smaller D_p, accompanied with a lower GR, is observed when adding a certain amount of polyethylene glycol to phosphoric acid. This additive increases the viscosity and decreases the acidity of the electrolyte mixtures, reducing D_p from 200 nm to 100 nm[11]. Other authors showed that, in glycerol solution of oxalic acid, the AAOs thicknesses are linearly dependent on the inverse of electrolyte viscosity[12], confirming the GR decrease when using more viscous electrolyte. On the contrary, ethanol and ionic liquids have been used to increase the GR. Qin et al. found that 10 % of ethanol can increase the GR by a factor of 5 with a D_p of 15 nm while keep-

ing the voltage low (25 V)[13]. However, the addition of more ethanol has the reverse effect, i.e. decrease the GR. Similarly Salerno et al. showed that the use of ionic liquids (from 0.01 to 1%v/v of 1-Butyl-3-methylimidazolium 2-(2-methoxyethoxy) ethyl sulfate and 1-Butyl-3-methylimidazolium tetrafluoborate) in 0.03 M oxalic acid under galvanostatic conditions also increases the GR by a factor of 3.5[14].

In this context, we propose an original approach for the AAO synthesis using deuterated solvent (heavy water, D_2O) and/or deuterated acids (such as deuterated sulfuric acid, D_2SO_4). The use of deuterated species has not been fully exploited, while it can provide valuable information, in particular on the structural AAO features. So far, few works involved deuterated species for AAOs synthesis[15, 16] and none investigated the morphologies of AAOs prepared with deuterated electrolytes but focused on the possible AAO hydration during the synthesis. Indeed, under the high electric field generated during the anodization, water dissociates in O^{2-} and/or OH^- migrating inside the oxide and forming with Al^{3+} alumina (Al_2O_3) or aluminum hydroxydes such as AlOOH (boehmite) or $Al(OH)_3$ (bayerite) depending on the OH^- quantity[17, 18]. By using deuterated species, one substitutes D for H and can probe the presence (or not) of D within the structure. Dorsey used deuterated electrolytes to elucidate the hydration of the anodic films by infrared absorption spectroscopy[15] probing shifts in bands to lower wavenumbers in AAOs synthesized in deuterated sulfuric acids. Lu and coworkers[16] studied the diffusion of H/D through the barrier layer in thin films synthesized on Si wafers by Secondary Ion Mass Spectroscopy and observed the deuterium incorporation into AAO and at the Si/AAO interface. In this pa-

per, we investigate the influence of deuterium (D) i) on the structural pore organization, morphology and GR and ii) gain understanding on the chemical composition (anion incorporation and possible hydration) of AAOs by coupling Energy Dispersive Spectroscopy (EDS) and Small Angle Neutron Scattering (SANS), the latter being very sensitive to deuteration substitution.

2. Experimental methods

2.1. AAOs preparation

Herein, AAOs are prepared using the classical two-step anodizations using different sulfuric or oxalic based electrolytes at a fixed concentration of 0.3 M: deuterated sulfuric acid in D_2O (named D_2SO_4/D_2O), hydrogenated sulfuric acid in D_2O (H_2SO_4/D_2O), hydrogenated sulfuric acid in H_2O (H_2SO_4/H_2O) and oxalic acid (OA, $H_2C_2O_4$) in H_2O or D_2O. Table S1 summarizes the different physical and chemical parameters of the different electrolytes used in this work. One can notice a pH increase and a conductivity decrease in D_2O, in good agreement with the weaker acid dissociation already observed in the literature. A first anodization is carried out during 2 hours (h) at a constant temperature (from 4^oC to 20^oC for sulfuric and 18^oC for oxalic electrolytes) and constant applied voltage (20 V and 40 V for sulfuric and oxalic acid, respectively). Note that the breakdown voltage was found to be 21 V in sulfuric/D_2O electrolyte while it is 27 V in sulfuric/H_2O. The formed oxide is then chemically dissolved in phosphochromic acid solution (6 wt% H_3PO_4 and 1.8 wt% CrO_3) during 2 h at 60^oC. Finally, a second anodization is performed under the same conditions as the first one during a chosen time

(typically from 1 h to 8 h).

2.2. Scanning Electron Microscopy (SEM) and Energy Dispersive spectroscopy (EDS)

The AAOs were characterized by Scanning Electron Microscopy (SEM) to access the pore morphology and ordering. SEM imaging were performed on a field emission gun scanning electron microscope (FEGSEM, SU-70 Hitachi) at an accelerating voltage of 3 kV and images with different magnifications (x10000, x20000, x50000 and x100000) have been recorded. Energy Dispersive spectroscopy (EDS) has been performed with an OXFORD X-Max SDD for elemental analysis (Al, O, C and S elements) at 5 kV on different areas of uncoated samples after calibration with a silicon standard.

2.3. Small-Angle Neutron Scattering (SANS)

Small-Angle Neutron Scattering (SANS) experiments have been performed on PAXY spectrometer (Laboratoire Léon Brillouin, LLB CEA Saclay) and D11 spectrometer (Institut Laue Langevin, ILL). On PAXY, four configurations were used: 6.7m/15Å, 5m/8.5Å, 3m/5Å, 1m/5Å covering a q range from 2.10^{-3} $Å^{-1}$ to 0.5 $Å^{-1}$ and data reduction was performed with homemade PASINET software. On D11, four configurations were used: 39m/6Å, 16m/6Å, 8m/6Å, 1.4m/6Å covering a q range from 2.10^{-3} $Å^{-1}$ to 0.4 $Å^{-1}$ (data available in ref[19]) and data reduction was performed with ILL GRASP software[20]. The AAOs are aligned along the neutron beam and immersed into H_2O/D_2O mixtures (73.2 % or 75.5 % D_2O) to avoid multiple scattering effects. We recently described a detailed methodology to measure AAOs by SANS[21] and here we will only provide the necessary information for the

basic understanding of the data interpretation. From SANS, we measure the scattering intensity I(q) from which information about the structure and chemical composition can be extracted through the complete fitting of the experimental data. The intensity depends on the averaged scattering amplitude of the object form <F(q)> and the structure factor S(q). For the latter, a hard sphere (HS) or hexagonal (HEX) model[22, 21] have been used depending on the degree of ordering. Then, the F(q) can be reproduced by a core/shell model, the core being the pore filled with the solvent and the shell being the contaminated layer (see below). The composition is accessed by the scattering length density (SLD, noted ρ in the model) that depends on the chemical formula and the density of the materials. In our recent work, we also pointed out the importance of the length implemented in the fitting model corresponding to the longitudinal correlation length L_z (which is not equivalent to the real AAO length). L_z is determined by measuring the scattering intensity variation at the Q_{10} peak position as a function of the tilting angle along the pore axis. By doing so we obtained a rocking curve from which L_z is calculated (see as an example in Figure S1 the rocking curve of AAO synthesized in OA/H_2O). In the following the SANS data will be presented with the best fits given by the model and the fitting parameters will be listed in a table.

3. Results and Discussion

3.1. Influence of deuterated electrolytes on structural organization and growth rate

3.1.1. Pore diameter and ordering

Fig.1a shows SEM images of AAOs top surface synthesized in D_2SO_4/D_2O, H_2SO_4/D_2O and H_2SO_4/H_2O at T=10 ^oC under 20 V during 8 h. Image analysis give similar pore densities but different mean D_p of 20 +/- 3 nm, 16 +/- 3 nm and 16 +/- 3 nm for H_2SO_4/H_2O, H_2SO_4/D_2O and D_2SO_4/D_2O, respectively, corresponding to a D_p decrease of around 20 % when using deuterated water with no significant changes in the pore diameter dispersity (see Table 1). The use of H_2SO_4 or D_2SO_4 with D_2O doesn't modify the D_p, indicating that even a small H content within the electrolyte doesn't influence the pore morphology. When anodizing during a shorter time (2 h) the D_ps are smaller (around 12.5 nm, see Fig. 1b) and remain similar whatever the electrolyte used, indicating that the pore dissolution is time and electrolyte dependent. The dissolution rate is enhanced in hydrogenated electrolyte after a long time (1.1 nm/h and 0.6 nm/h for H_2SO_4/H_2O and D_2SO_4/D_2O, respectively) and this effect is attributed to a stronger acidity of the hydrogenated electrolyte (i.e. having more H^+, see pH and conductivity values in Table S1).

Moreover, if we focus on D_2SO_4/D_2O electrolytes, the SEM images analysis showed a slight increase of pore diameter up to 15^{o}C and a more pronounced increase at 20^{o}C (Fig. 1c, blue squares). More interestingly one can reach a D_p of 11 +/- 3 nm for 1 h anodization, reaching a pore size similar to the smallest ones obtained up to now by using selenic acid[8] but with a higher aspect ratio and pore density, structural features very interesting for

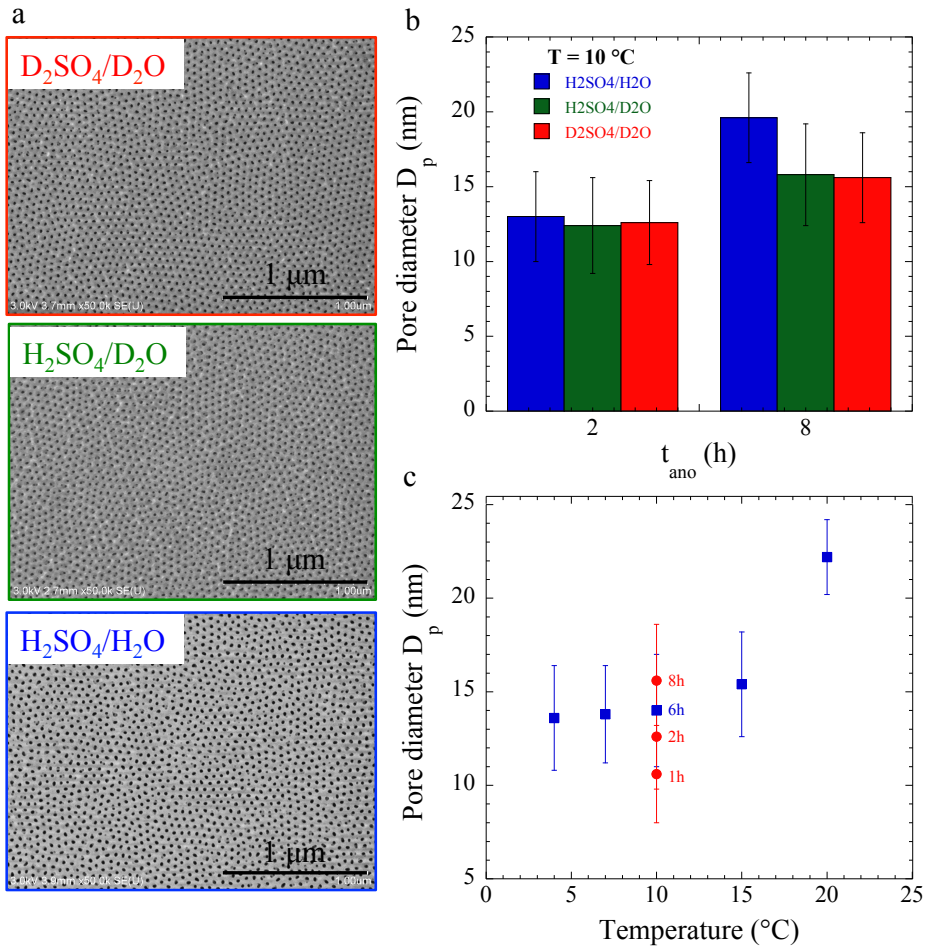

Figure 1: SEM images of AAO top surface prepared with D_2SO_4/D_2O (red), H_2SO_4/D_2O (green) and H_2SO_4/H_2O (blue). Scale bar: 1 μm. (b) Pore diameter D_p for the three systems after 2 h and 8 h anodization. (c) D_p evolution with temperature at a given anodization time (6 h, blue squares) and with time at a given temperature (10 ^{o}C, red circles) for AAOs synthesized in D_2SO_4/D_2O.

Table 1: Structural parameters obtained from SEM analysis (pore size distribution and S(q)) of the AAOs synthesized in sulfuric electrolytes during 8 h and oxalic electrolytes during 11h30: pore diameter D_p, length L (one side), pore density n, porosity, interpore distance D_{int}, D_{int} standard deviation σ_{int}, grain size D. * For H_2SO_4/H_2O the S(q) is fitted with a hard sphere model giving an ordering parameter η. Also the grain size cannot be determined with this model (NA = Non Available).

Electrolytes	H_2SO_4/H_2O	H_2SO_4/D_2O	D_2SO_4/D_2O	OA/H_2O	OA/D_2O
j ($mA.cm^{-2}$)	1.7	2.6	2.9	4.0	3.2
D_p (nm)	20 +/- 3	16 +/- 3	16 +/- 3	55 +/- 3	44 +/- 3
L (μm)	23	27	36	84	60
GR (μm/h)	2.9	3.4	4.5	7.3	5.2
n (10^{10} cm^{-2})	4.4	4.5	4.2	1.1	1.1
Porosity (%)	16	12	9	26	16
D_{int} (nm)	52.6	52.8	52.7	100	103
η^* / σ_{int}	0.49 / -	- / 0.098	- / 0.084	- / 0.06	- / 0.06
Grain size (nm)	NA	314	370	714	997

applications such as molecular filtration or the preparation of nanostructures by templating approach[23].

Then, the pore ordering is quantified by performing the 2D Fast Fourrier Transform (FFT) of the pore centers in order to compute the structure factor S(q) as shown in Fig.2a for H_2SO_4/H_2O (blue), H_2SO_4/D_2O (green) and D_2SO_4/D_2O (red). The S(q) gives information about the pore ordering and can be reproduced by different models depending on the ordering degree (see reference [21] for complete mathematical expressions). The S(q) of AAOs synthesized in D_2O show clear peaks at intermediate q (q_{11} and q_{20}) coming from a better pore organization and can be fitted with a 2D hexagonal model.

On the contrary the S(q) of AAOs synthesized in H_2O cannot be reproduced by the same model and is fitted with a hard sphere model indicating that the pores adopt a more disordered organization (the fitting parameters are also listed in Table 1). A hexagonal grain size cannot be extracted in H_2O while a transverse hexagonal domain size of 370 nm is obtained in D_2O. Focusing only on the D_2SO_4/D_2O AAOs synthesized at different temperatures, the S(q) analysis in Fig.2b shows quite similar ordering between 4 ^oC and 15 ^oC and a slightly better ordering at 20 ^oC (smaller σ_{int} and a larger grain size, see Table S2). We can also notice that the anodization time (up to 8 h) doesn't modify the ordering as observed recently for AAOs prepared with oxalic acid[21].

Similar analyses have been performed for AAOs synthesized in 0.3 M OA. Fig.3a and 3b show the SEM images of AAOs prepared in H_2O and D_2O, respectively, and Fig.3c shows the corresponding S(q) derived from the images analysis and both fitted with an hexagonal model. Similar trends are observed in oxalic electrolyte: D_p decreases by around 20 % in D_2O (from 55 nm in H_2O to 44 nm in D_2O) and the grain size increases from 714 nm in H_2O to 997 nm in D_2O (around 40 % increase, see Table 1).

First, it has been observed that the best self-ordered pore structure is obtained for anodization performed just below the breakdown potential U_B, corresponding to the voltage at which burning phenomena occur[24]. U_B depends on the anodized metal (here Al), current density, electrolyte resistivity and composition of the oxide[6]. For H_2SO_4/H_2O, U_B = 27 V and, in this work, we experimentally found that in D_2O U_B = 21 V, close to our applied voltage of 20 V. The apparent increase of ordering can be related to

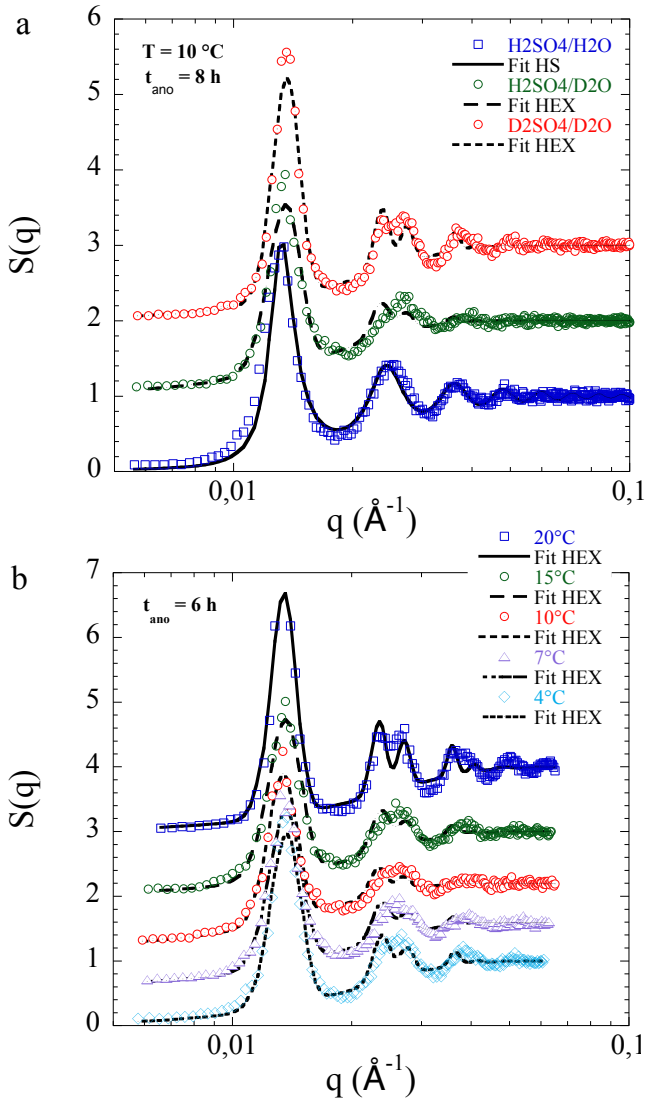

Figure 2: (a) Structure factor S(q) derived from the SEM images analysis fitted with hard sphere model in H_2SO_4/H_2O and a hexagonal model for H_2SO_4/D_2O and D_2SO_4/D_2O (AAOs are synthesized during 8 h at 10 ^{o}C). The curves have been shifted vertically for clarity. (b) Structure factor S(q) derived from the SEM images analysis of AAOs prepared in D_2SO_4/D_2O at different temperatures with the corresponding hexagonal fits (anodization time of 6 h). The SEM images are shown in Figure S2.

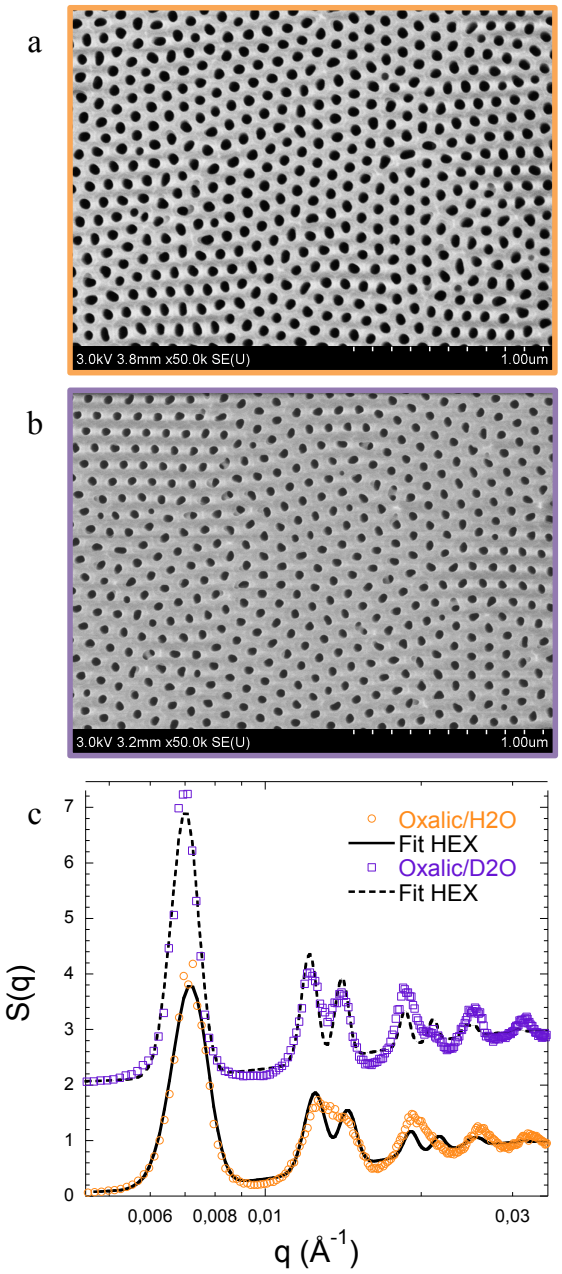

Figure 3: SEM images of AAOs synthesized with OA in (a) H_2O and (b) D_2O. (c) S(q) derived from SEM analysis. The black lines correspond to the best hexagonal fits. The S(q) in D_2O has been shifted for clarity.

Table 2: Anion incorporation determined by EDS measurements.

Electrolytes	H_2SO_4/H_2O	H_2SO_4/D_2O	D_2SO_4/D_2O	OA/H_2O	OA/D_2O
S/Al	0.071+/-0.004	0.091+/-0.005	0.105+/-0.004	≈ 0	≈ 0
C/Al	0.037+/-0.006	0.036+/-0.005	0.0245+/-0.0004	0.100+/-0.008	0.14+/-0.01
Grain size (nm)	NA	314	370	714	997

the convergence of U_B to our working voltage.

Second, the increase in ordering can also be correlated to the incorporation of anions coming from the electrolyte during the anodization (sulfates or oxalates for sulfuric or oxalic acid respectively)[25]. Indeed, during the AAO growth, compressive stress arises at the oxide/electrolyte interface due to the incorporation of anions, which in turn produces tensile stress at the oxide/metal interface, causing the oxide plastic flow from the pore bottom to the pore surface[26] and finally influencing the pore self-ordering. Thus anion incorporation plays an important role: self-ordering increases when incorporation increases. In this context, we used Energy Dispersive Spectroscopy (EDS) to determine the incorporation level in AAOs, i.e. the S/Al and C/Al ratios for sulfuric and oxalic AAOs, respectively. To quantify the amount of S or C coming from external contamination (i.e. not from incorporation during the synthesis) we measure the S content of oxalic samples (where normally there is no S) and the C content of sulfuric samples (where normally there is no C). Table 2 shows the results. First, there is no S external contamination since none is measured in oxalic samples. However there is a C external contamination estimated around a C/Al of 0.033. Then a clear increase of S/Al or C/Al is observed when D_2O is used as a solvent, indicating an increase of anion incorporations correlated with the increase in grain size.

3.1.2. Influence on the growth rate (GR)

Now we will study the effect of D_2O on the pore growth rate (GR, calculated from the AAO thickness obtained by cross section SEM images). In particular the GR can be explored through the current density j, modified here by changing the temperature or the voltage. Fig.4 shows the GR evolution with j for sulfuric (Fig. 4a) and OA (Fig. 4b) electrolytes prepared in H_2O and D_2O. For all electrolytes, the GR is linear with j but different values of the slopes (given in Fig. 4a and 4b) are obtained depending on the solvent (H_2O or D_2O) or the nature of the electrolyte (sulfuric or OA). For sulfuric acid, the GR is larger in deuterated electrolytes (around 25 % higher for D_2SO_4/D_2O), while there is no clear deuterated effect for oxalic electrolytes. To gain more understanding, the GR evolution can be discussed in relation with the activation energy E_a of the reaction process, i.e. aluminum oxidation during the first anodization. The E_a is obtained by fitting the j versus 1/T plot (see Figure S3, the voltage is fixed to 20 V for sulfuric and 40 V for OA) with the following Arrhenius equation:

$$j = j_0.exp(-\frac{E_a}{RT}) \quad (1)$$

For sulfuric electrolytes, one finds an E_a of 52 +/- 3, 47+/- 5 and 41 +/- 3 kJ.mol^{-1} for H_2SO_4/H_2O, H_2SO_4/D_2O and D_2SO_4/D_2O, respectively. Thus an increase in GR can be correlated with a decrease in E_a when using D_2O as a solvent. For OA, the E_a remains quite similar between H_2O and D_2O: one gets an E_a of 46 +/- 3 and 50 +/- 5 kJ.mol^{-1} for OA/H_2O and

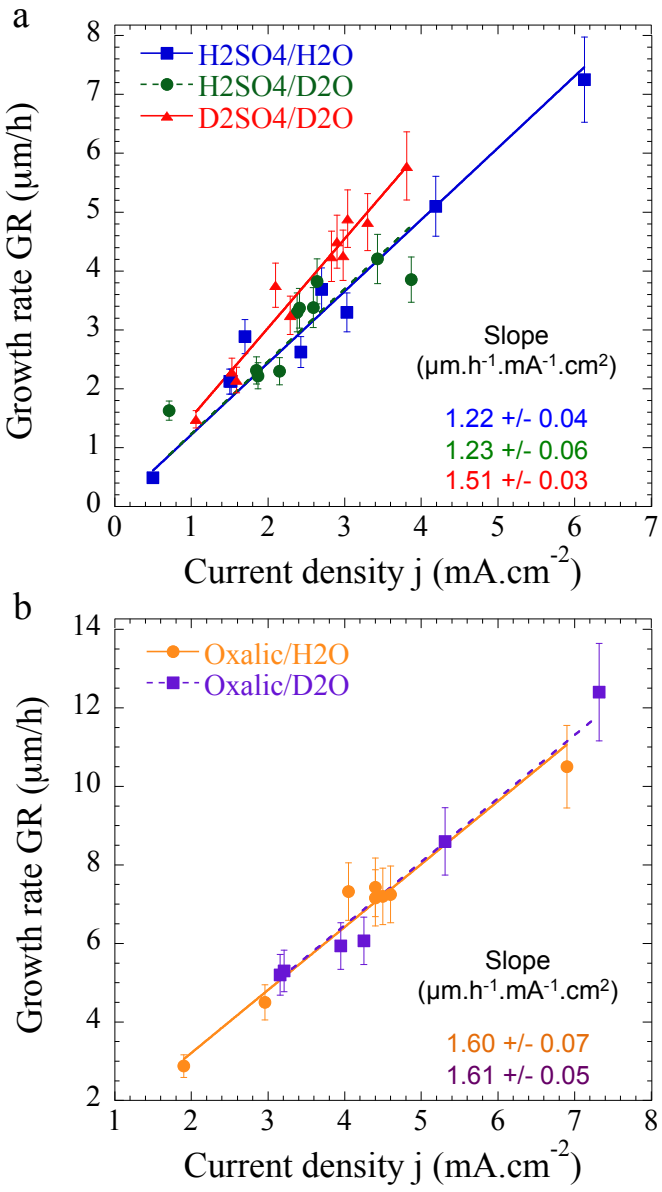

Figure 4: Growth rate (GR) as a function of the average current density j for (a) AAOs synthesized in H_2SO_4/H_2O (blue squares), H_2SO_4/D_2O (green circles) and D_2SO_4/D_2O (red triangles) and (b) for AAOs synthesized in OA/H_2O (orange circles) and OA/D_2O (purple squares).

OA/D_2O, respectively, which is coherent with the similar GR values. It has to be noticed that for both electrolytes, the conductivity decreases in D_2O (see Table S1), suggesting that the growth of AAOs in deuterated electrolyte is always more efficient.

From all the different structural aspects we presented, it is clear that deuterated electrolytes modify some important AAO structural features and can be thus an interesting alternative for the synthesis of AAOs with specific morphologies. It is known that the dissociation constants of acids are modified in D_2O (because D_2O has different physical properties such as a higher viscosity)[27]. Such differences have effects on the pore structure: for example, a lower acidity in D_2O leads to smaller pore diameters (as low as the smallest values observed in the literature so far). However, other observations made in D_2O cannot be fully understood: the increase of anion incorporation and the increase in GR for sulfuric suppose that D_2O has a complex influence on the growth mechanism which is electrolyte dependent (here sulfuric and OA don't show the same effect on the GR). Alumina is obtained by the reaction of aluminium ions Al^{3+} coming from the Al oxidation with oxygen ions coming from water dissociation. The water dissociation rate under electric field, i.e. the rate for providing O^{2-} or OH^- to form alumina, is a determining parameter that controls several processes in the AAO formation[28] such as the migration of anionic species within the material and a modification of such water dissociation in D_2O might explain our results[29]. So far, no studies investigated such influence on AAOs but recent work reported clear electrochemical effects of isotopic substitution[30].

3.2. Investigation of OH incorporation and AAO aging by SANS

3.2.1. OH incorporation in AAO

The synthesis in deuterated electrolytes also allows to elucidate the presence of H within the AAOs due to the incorporation of OH^- during the synthesis. The OH quantity can be determined by thermogravimetric measurements (TGA). Mata-Zamora et al.[31] investigated by TGA AAOs prepared in aqueous electrolytes of sulfuric, oxalic or phosphoric acid and proposed empirical chemical formulas having the following general expression: $(Al_2O_{3-x})(anion)_a(OH)_b$ (anions being sulfates, oxalates or phosphates depending on the electrolyte nature). They found that AAOs prepared in sulfuric acid contained more OH and anions relative to the ones prepared in phosphoric or oxalic acid. However the total OH amount remains low (b= 0.08, 0.04 and 0.001 for sulfuric, oxalic and phosphoric, respectively) indicating a weak OH incorporation. Then TGA cannot discriminate between surface OH and trapped OH inside the AAO. To solve this issue, O'Sullivan conducted FTIR measurements under D_2O atmosphere and quantified the H/D exchange. They observed that all OH groups are available for H/D exchange suggesting that hydroxyl groups are located at the surface and not trapped inside the materials[32].

Here, the synthesis in D_2O can provide further information about the OH incorporation. Indeed, such presence in the structure can be revealed by substituting D for H during the synthesis by the use of D_2O and then performing Small-Angle Neutron Scattering (SANS). SANS is a technique very sensitive to deuteration since atoms H and D have very different neutron scattering length b (b_H = -0.374x10^{-12} cm and b_D = 0.667x10^{-12} cm). As

mentioned in the experimental section, the chemical composition is given in SANS by the scattering length density (SLD, noted ρ) values, which are obtained by the fitting of the SANS data[21] and depend on the chemical formula and the density of the material as follows:

$$\rho = \frac{dN_a}{M} \sum_i b_i \tag{2}$$

With d the density, N_a the Avogadro number, M the molecular weight and b_i the scattering length of atom i. Thus, a difference in SLD can be explained by a difference in composition or by a difference in the density of the materials. As a consequence, the comparison of the SLD values of hydrogenated and deuterated AAOs will reveal the OH incorporation of alumina: if AAO contains OH groups then the differences between AAOs synthesized in H_2O or D_2O will be observed. On the contrary, if there is no H (or if the H quantity is too low to be detected) then the SLDs will be similar. The sensitivity can be evaluated by estimating the expected SLD values. With the empirical formulas proposed by Mata-Zamora[31] one can calculate the AAO SLD and, by substituting D for H and assuming a similar density (3 $g.cm^{-3}$), the expected SLD for AAO synthesized in deuterated electrolytes. One finds 4.24x10^{-6} $Å^{-2}$ and 4.36x10^{-6} $Å^{-2}$ for AAOs synthesized in H_2O and D_2O, respectively. The difference (around 3 %) is detectable by SANS due to the high AAO scattering, the error bars of the SLD values extracted from the data fitting lie on the second digits[21] .

Figure 5a and 5b shows the scattering intensities of AAOs synthesized in H_2SO_4/H_2O (blue circles) and D_2SO_4/D_2O (red squares) measured in 73.2 % and 75.5 % D_2O, respectively. As explained in the experimental sec-

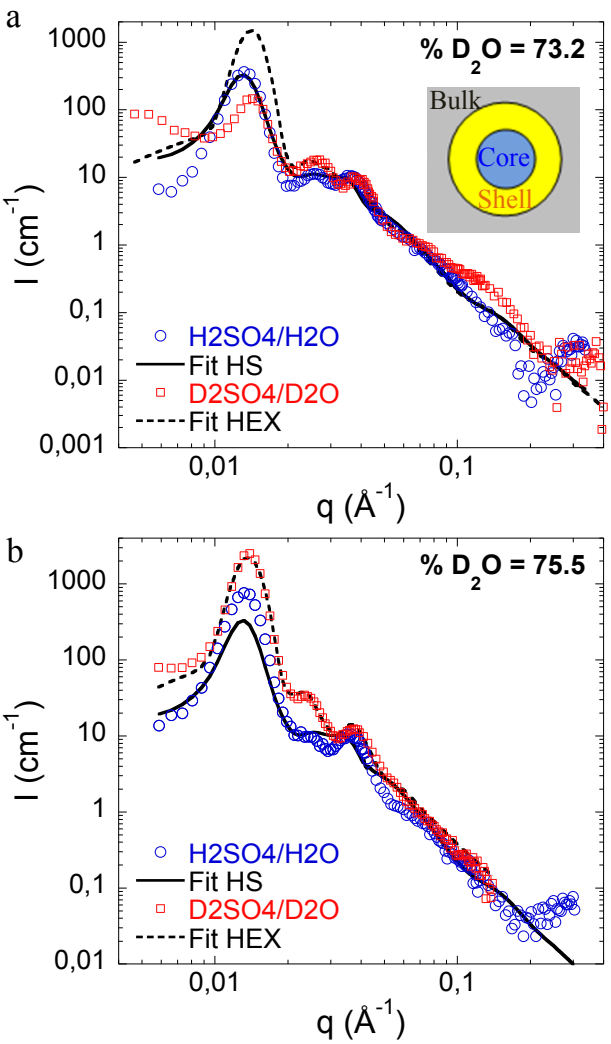

Figure 5: (a) SANS scattering intensities of AAOs synthesized in H_2SO_4/H_2O (blue circles) and D_2SO_4/D_2O (red squares) measured in (a) 73.2 % and (b) 75.5 % D_2O. The continuous and dashed lines correspond to the best fit. The scheme inserted in (a) represents the core/shell model used to fit the data.

tion, the data have been fitted with a model combining an aligned core/shell cylinder form factor (depicted in insert of Fig. 5a) and a hard sphere or hexagonal structure factor. All the details of this model are fully described in our previous work[21] and Table 3 lists all the fitting parameters. This model nicely reproduced the experimental data (except for the first peak of the D_2SO_4/D_2O AAOs in 73.2 % D_2O, this discrepancy being attributed to possible micro cracks adding a Porod contribution at low q and different information can be extracted:

i) SANS measurements confirms the better ordering of the D_2SO_4/D_2O AAOs: the longitudinal correlation length L_z, corresponding to an ordering length in the longitudinal direction, is larger for D_2SO_4/D_2O (4.43 μm) than the H_2SO_4/H_2O (1.74 μm).

ii) as for AAOs prepared in OA[21], the AAOs made in sulfuric acid are not homogenous in composition, the SANS cannot be fitted without a contaminated shell of 5.2 nm and 6.3 nm for H_2SO_4/H_2O and D_2SO_4/D_2O, respectively. The composition of the shell will be discussed with the SLD below.

iii) since the same structural parameters have been used for the fitting of the 73.2 % and 75.5 % D_2O, more reliable SLD values are obtained by averaging the shell and bulk SLD determined for both contrasts. The SLDs gives information about the AAOs chemical composition and its possible hydration. One obtains ρ_{shell} = (4.61 +/- 0.09)x10^{-6} Å^{-2} and ρ_{bulk} = (4.49 +/- 0.09)x10^{-6} Å^{-2} for H_2SO_4/H_2O and ρ_{shell} = (4.59 +/- 0.08)x10^{-6} Å^{-2} and ρ_{bulk} = (4.50 +/- 0.07)x10^{-6} Å^{-2} for D_2SO_4/D_2O. The ρ_{shell} is higher than ρ_{bulk} suggesting the incorporation in the shell of elements increasing the

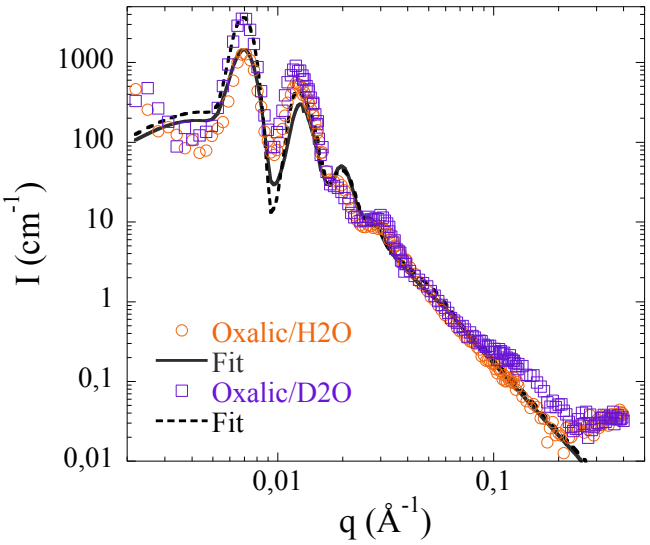

Figure 6: SANS scattering intensities of AAOs synthesized in OA/H_2O (orange circles) and OA/D_2O (purple squares). The continuous and dashed lines correspond to the best fit.

SLD (such as S), in good agreement with the previous EDS characterization. However, no differences in SLD are observed when comparing deuterated and hydrogenated electrolytes. As mentioned previously, the SLDs depend on a combined effect of density and chemical composition. In D_2O, an increase in anion incorporation (increasing the SLD) is accompanied with a decrease in density (decreasing the SLD), leading to comparable SLD values as in H_2O. In addition, our results suggest that the OH or OD incorporation during the synthesis is very weak and not detected by SANS.

Similarly, SANS of AAOs synthesized in OA doesn't show drastic differences between H_2O and D_2O as seen in Figure 6 where the SANS data superimpose; the small differences are due to the better ordering in D_2O (see fitting parameters in Table 3). The SLD values obtained by the fit are

Table 3: Parameters obtained by the fitting of SANS data in Figure 4. See reference[21] for full details. The * refers to fixed parameters during the SANS fitting. [a] For H_2SO_4/H_2O, a HS model has been used for the S(q).

Name	H_2SO_4/H_2O[a]	H_2SO_4/H_2O[a]	D_2SO_4/D_2O	D_2SO_4/D_2O	OA/H_2O	OA/D_2O	F(q) or S(q)
% D_2O	75.5	73.2	75.5	73.2	73.2	73.2	-
D_{int} (nm)	52.6	52.6	51.5	50	97.5	102	S(q)
σ_a	-	-	0.084	0.084	0.061	0.058	S(q)
δ (x 10^{-4} Å^{-1})	0.49	0.49	17	17	8.8	6	S(q)
c_L	-	-	24.2	30	12	13	S(q)
$*\phi_s$	0.35	0.35	0.27	0.27	0.62	0.58	F(q)
$*\rho_{solv}$ (10^{-6} Å^{-2})	4.65	4.52	4.65	4.52	4.52	4.52	F(q)
ρ_{shell} (10^{-6} Å^{-2})	4.68	4.55	4.65	4.54	4.54	4.53	F(q)
ρ_{bulk} (10^{-6} Å^{-2})	4.55	4.42	4.55	4.45	4.43	4.45	F(q)
$*R_p$ (nm)	10	10	8	8	27.5	23.5	F(q)
σ_p	0.2	0.2	0.19	0.19	0.06	0.07	F(q)
t (nm)	5.8	5.7	6.3	6.3	15	17.5	F(q)
$*\sigma_t$	0.1	0.1	0.1	0.1	0.2	0.1	F(q)
$*L_z$ (μm)	1.74	1.74	4.43	4.43	2.28	3.62	F(q)

similar for H_2O and D_2O suggesting again an absence or a weak OH or OD incorporation, also confirmed by similar FTIR measurements (see Figure S4). Our results are consistent with the observations of O'Sullivan et al.[32] who concluded that no OH are trapped in the materials but are at the surface. One can imagine that surface OD groups are present after the synthesis in deuterated electrolytes and that further H/D exchange occurs with the H_2O molecules of the solvent mixture used for SANS measurements.

3.2.2. AAO aging in H_2O and D_2O

Finally, we propose to follow the AAO aging after a long immersion in H_2O or D_2O at room temperature. It has been observed that, in water,

alumina transforms into aluminum hydroxydes boehmite (AlOOH) or more probably bayerite ($Al(OH)_3$), such transformation being thermodynamically favored but kinetically slow[33]. Such process induces at the AAO surface a pore sealing, an interesting property for applications involving corrosion resistance. Here, we aim in particular at studying the effect of D_2O on this sealing process.

Pieces of AAO synthesized in OA/H_2O are immersed in H_2O or D_2O during 30 days at room temperature. These samples are then measured by SANS in 73.2 % D_2O mixture. Figure 7a shows the SANS spectra after immersing the AAO 30 days in H_2O (green squares) or D_2O (red circles). For comparison we also plotted the SANS signal of the "as prepared" sample, i.e. AAO that has not been immersed[21]. First, compared to the as prepared AAO, the whole scattering intensities of "immersed" AAOs are shifted vertically after the immersion both in H_2O or D_2O. Second, the amplitudes of the different peaks at low q are also modified with an increase of the first peak more pronounced after immersion in H_2O than in D_2O and high incoherent plateaus are clearly visible at high q with similar levels for AAOs immersed in H_2O and D_2O. All these modifications in the SANS curves indicates changes in the AAO composition. Further data fitting also shown in Figure 7a provides the results presented in Table 4. One can notice that the pore hexagonal organization and radius are barely affected by the aging but the shell and bulk SLD values decrease in both cases, this decrease being more pronounced after immersion in H_2O. In the case of AAO immersed in H_2O, such SLD decrease is consistent with the alumina transformation into aluminum hydroxyde (bayerite), i.e. with the presence of H in the material.

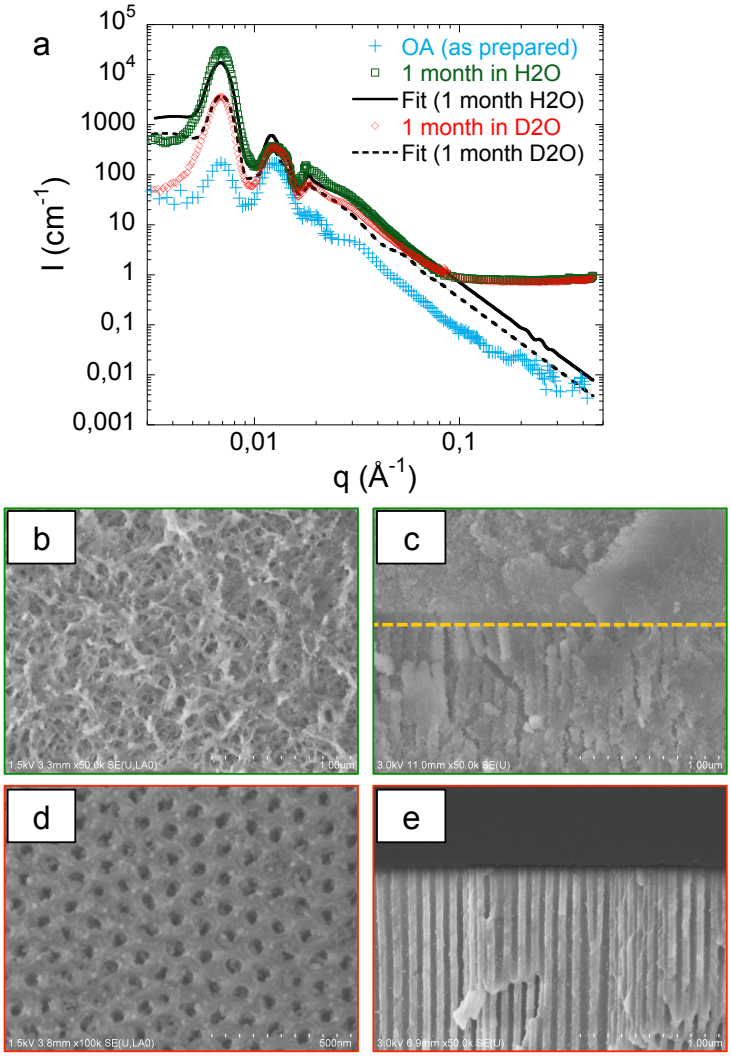

Figure 7: (a) SANS scattering intensities of AAOs synthesized in OA/H_2O measured in 73.2 D_2O as prepared (blue crosses), after immersion in H_2O (green squares) and D_2O (red circles). The continuous and dashed lines correspond to the best fit. The as prepared AAO has already been fitted in our previous work[21].(b, c, d, e) Top and section SEM images of AAO synthesized in OA/H_2O after 30 days immersion in H_2O (b, c) or D_2O (d, e).

Table 4: Parameters obtained by the fitting of SANS data in Figure 7. See reference[21] for full details. The * refers to fixed parameters during the SANS fitting. These samples were measured in 73.2 % D_2O mixture. The as prepared AAO has already been fitted in our previous work.[21].

Name	As prepared	1 month in H_2O	1 month in D_2O
D_{int} (nm)	100	103	101
σ_a	0.06	0.06	0.06
δ (x 10^{-4} Å^{-1})	9.5	7	7
c_L	10	10	10
$*\phi_s$	0.56	0.67	0.79
$*\rho_{solv}$ (10^{-6} Å^{-2})	4.52	4.52	4.52
ρ_{shell} (10^{-6} Å^{-2})	4.58	4.40	4.48
ρ_{bulk} (10^{-6} Å^{-2})	4.50	4.12	4.28
$*R_p$ (nm)	26.7	26.7	26.7
σ_p	0.14	0.25	0.25
t (nm)	15	19	23
σ_t	0.1	0.2	0.1
$*L_z$ (μm)	1.33	1.33	1.33

In the case AAO immersed in D_2O, one can propose the same transformation with the presence of D in the AAO. However, deuterium should increase the SLD values while a SLD decrease is measured, suggesting H/D exchange during the SANS measurement.

To go further we performed SEM to confirm the SANS analysis. Figures 7b, c, d, e show top and section view of AAO immersed in H_2O (b, c) and D_2O (d, e). For AAO immersed in H_2O the pores are not anymore

visible on the top surface (Fig. 7b), confirming the alumina transformation and pore sealing. However this sealing only affects the top surface, as seen on the SEM section view (Fig. 7c) where nanochannels are still present below a non-porous layer. On the contrary, for AAO immersed in D_2O, there is no non-porous layer on the top surface (Fig. 7d, e), the pores are still visible. O'Sullivan et al. speculated that hydrothermal AAO treatment doesn't modify the AAO bulk composition but induces a pore sealing[32]. Here, we show by combining SANS and SEM that aging in water affects the AAO composition, even before the pore sealing (see aging in D_2O where no sealing is observed but SLDs values changed). Additionally, our results clearly evidence a much slower kinetic of alumina transformation in D_2O.

4. Conclusion

In this paper we proposed an experimental alternative to synthesize AAOs with interesting structural features by using deuterated electrolytes. The use of D_2O leads to the formation of smaller pores with an improved hexagonal ordering. The pore diameter reached with deuterated electrolytes is as small as the smallest pore size obtained so far in the literature. Moreover, for sulfuric electrolytes, an increase in GR is observed and related to a decrease of the activation energy of aluminum oxidation. Additionally, deuterated electrolytes allow to quantify the possible OH incorporation in AAOs during the synthesis by the use of SANS. SANS measurements don't show drastic changes between hydrogenated and deuterated AAOs suggesting a weak OH incorporation. Finally, the AAO aging in H_2O or D_2O has also been investigated and our results shows that the alumina transformation is kinetically

slower in D_2O. This work provides an efficient opportunities to synthesize AAOs with specific morphologies and brings new fundamental insight into the effect of deuterated species in the synthesis and properties of nanoporous materials.

5. Acknowledgements

The authors thank the Institut des Matériaux de Paris Centre (IMPC FR2482) for servicing FEGSEM and EDX instrumentation and Sorbonne Université, CNRS and C'Nano projects of the Région Ile-de-France for his funding and we thank David Montero for his help during the SEM characterization. We also thank Lionel Porcar for his help during the SANS experiments on D11 at ILL. Laboratoire Léon Brillouin (LLB) and Institut Laue Langevin (ILL) are acknowledged for beamtime allocation.

References

[1] P. Huber, Soft matter in hard confinement: phase transition thermodynamics, structure, texture, diffusion and flow in nanoporous media, Journal of Physics-Condensed Matter 27 (10) (2015) 103102.

[2] F. Tian, J. Lyu, J. Shi, F. Tan, M. Yang, A polymeric microfluidic device integrated with nanoporous alumina membranes for simultaneous detection of multiple foodborne pathogens, Sensors and Actuators B: Chemical 225 (2016) 312–318.

[3] C. T. Sousa, D. C. Leitao, M. P. Proenca, J. Ventura, A. M. Pereira, J. P. Araujo, Nanoporous alumina as templates for multifunctional applications, Applied Physics Reviews 1 (3) (2014) 031102.

[4] H. Masuda, K. Fukuda, Ordered metal nanohole arrays made by a two-step replication of honeycomb structures of anodic alumina, Science 268 (1995) 1466–1468.

[5] W. Lee, R. Ji, U. Gosele, K. Nielsch, Fast fabrication of long-range ordered porous alumina membranes by hard anodization, Nat Mater 5 (9) (2006) 741–747, 10.1038/nmat1717.

[6] W. Lee, S. J. Park, Porous anodic aluminum oxide: Anodization and templated synthesis of functional nanostructures, Chemical Reviews 114 (15) (2014) 7487–7556.

[7] S. Ono, M. Saito, H. Asoh, Self-ordering of anodic porous alumina formed in organic acid electrolytes, Electrochimica Acta 51 (5) (2005) 827–833.

[8] O. Nishinaga, T. Kikuchi, S. Natsui, R. O. Suzuki, Rapid fabrication of self-ordered porous alumina with 10-/sub-10-nm-scale nanostructures by selenic acid anodizing, Scientific Reports 3 (2013) 2748.

[9] J. Martin, C. V. Manzano, O. Caballero-Calero, M. Martin-Gonzalez, High-aspect-ratio and highly ordered 15-nm porous alumina templates, Acs Applied Materials and Interfaces 5 (1) (2013) 72–79.

[10] C. Cheng, K. Ng, A. Ngan, Quantitative characterization of acid concentration and temperature dependent self-ordering conditions of anodic porous alumina, AIP Advances 1 (4) (2011) 042113.

[11] W. Chen, J.-S. Wu, X.-H. Xia, Porous anodic alumina with continuously manipulated pore/cell size, ACS Nano 2 (5) (2008) 959–965.

[12] W. J. Stepniowski, D. Forbot, M. Norek, M. Michalska-Domanska, A. Król, The impact of viscosity of the electrolyte on the formation of nanoporous anodic aluminum oxide, Electrochimica Acta 133 (2014) 57–64.

[13] X. Qin, J. Zhang, X. Meng, L. Wang, C. Deng, G. Ding, H. Zeng, X. Xu, Effect of ethanol on the fabrication of porous anodic alumina in sulfuric acid, Surface and Coatings Technology 254 (2014) 398–401.

[14] M. Salerno, N. Patra, R. Losso, R. Cingolani, Increased growth rate of anodic porous alumina by use of ionic liquid as electrolyte additive, Materials Letters 63 (21) (2009) 1826–1829.

[15] G. Dorsey, The characterization of anodic aluminas iii. barrier layer composition and structure, Journal of The Electrochemical Society 113 (3) (1966) 284–286.

[16] P. H. D. Lu, H. Strutzberg, S. Wenham, A. Lennon, Hydrogen incorporation during aluminium anodisation on silicon wafer surfaces, Electrochimica Acta 133 (2014) 153–160.

[17] T. P. Hoar, N. F. Mott, A mechanism for the formation of porous anodic oxide films on aluminium, Journal of Physics and Chemistry of Solids 9 (2) (1959) 97–99.

[18] I. Farnan, R. Dupree, A. J. Forty, Y. S. Jeong, G. E. Thompson, G. C. Wood, Structural information about amorphous anodic alumina from 27al mas nmr, Philosophical Magazine Letters 59 (4) (1989) 189–195.

[19] N. Jouault, A. Chennevière, A. Christoulaki, E. Dubois, L. Porcar, Polyelectrolytes chain conformation under confinement: electrostatic effects studied by zero average contrast method. institut laue-langevin (ill), https://doi.org/10.5291/ill-data.9-11-1764 (2016).

[20] C. D. Dewhurst, Graphical reduction and analysis sans program for matlabtm, https://www.ill.eu/users/scientific-groups/large-scale-structures/grasp/.

[21] A. Christoulaki, A. Chenneviere, I. Grillo, L. Porcar, E. Dubois, N. Jouault, A novel methodology to study nanoporous alumina by small-angle neutron scattering, Journal of Applied Crystallography 52 (4) (2019) 745–754.

[22] S. Förster, A. Timmann, M. Konrad, C. Schellbach, A. Meyer, S. S. Funari, P. Mulvaney, R. Knott, Scattering curves of ordered mesoscopic materials, The Journal of Physical Chemistry B 109 (4) (2005) 1347–1360.

[23] S. J. Hurst, E. K. Payne, L. Qin, C. A. Mirkin, Multisegmented one-dimensional nanorods prepared by hard-template synthetic methods, Angewandte Chemie International Edition 45 (17) (2006) 2672–2692.

[24] S. Chu, K. Wada, S. Inoue, M. Isogai, A. Yasumori, Fabrication of ideally ordered nanoporous alumina films and integrated alumina nanotubule arrays by high?field anodization, Advanced Materials 17 (17) (2005) 2115–2119.

[25] I. Mínguez-Bacho, S. Rodríguez-López, A. Climent, D. Fichou, M. Vázquez, M. Hernández-Vélez, Influence of sulfur incorporation into nanoporous anodic alumina on the volume expansion and self-ordering degree, The Journal of Physical Chemistry C 119 (49) (2015) 27392–27400.

[26] J. E. Houser, K. R. Hebert, The role of viscous flow of oxide in the growth of self-ordered porous anodic alumina films, Nat Mater 8 (5) (2009) 415–420, 10.1038/nmat2423.

[27] W. P. Jencks, K. Salvesen, Equilibrium deuterium isotope effects on the ionization of thiol acids, Journal of the American Chemical Society 93 (18) (1971) 4433–4436.

[28] Z. Su, M. Bühl, W. Zhou, Dissociation of water during formation of anodic aluminum oxide, Journal of the American Chemical Society 131 (24) (2009) 8697–8702.

[29] J. J. Katz, Chemical and biological studies with deuterium, American Scientist 48 (4) (1960) 544–580.

[30] S. Cai, T. Bai, H. Chen, W. Fang, Z. Xu, H. Lai, T. Huang, H. Xu, X. Chu, J. Ling, C. Gao, Heavy water enables high-voltage aqueous electrochemistry via the deuterium isotope effect, The Journal of Physical Chemistry Letters 11 (1) (2020) 303–310.

[31] M. Mata-Zamora, J. Saniger, Thermal evolution of porous anodic aluminas: a comparative study, Revista mexicana de física 51 (5) (2005) 502–509.

[32] J. O'sullivan, J. Hockey, G. Wood, Infra-red spectroscopic study of anodic alumina films, Transactions of the Faraday Society 65 (1969) 535–541.

[33] X. Carrier, E. Marceau, J.-F. Lambert, M. Che, Transformations of γ-alumina in aqueous suspensions: 1. alumina chemical weathering studied as a function of ph, Journal of Colloid and Interface Science 308 (2) (2007) 429–437.